Available online at www.sciencedirect.com
SCIENCE DIRECT®
Journal of Solid State Chemistry 178 (2005) 2117–2127
JOURNAL OF SOLID STATE CHEMISTRY
www.elsevier.com/locate/jssc

Full potential linearized augmented plane wave calculations of positronic and electronic charge densities of zinc-blende AlN, InN and their alloy $Al_{0.5}In_{0.5}N$

Z. Bousahla, B. Abbar*, B. Bouhafs, A. Tadjer

Computational Materials Science Laboratory, University Research Centre, University of Sidi Bel-abbe's, Algeria

Received 6 December 2004; received in revised form 23 March 2005; accepted 29 March 2005

Abstract

A theoretical study of electron and positron band structures of zinc-blende AlN and InN and their alloy $Al_{0.5}In_{0.5}N$ is presented using the first-principles full-potential linearized augmented plane-wave method. Equilibrium lattices constants are determined from the total-energy minimization method. The results are compared with previous calculations and with experimental measurement. Electron and positron charge densities are computed as function of position in the unit cell. Detailed plots of distributions are along the $\langle 111 \rangle$ direction. The ionicity factors are calculated by means of three different approaches. The calculated results of the positron charge density reflect the high insight for the annihilation effect.

Keywords: Ab initio calculations; Positron and electron charge densities

1. Introduction

The lack of blue luminescent semi-conducting materials is still a problem for opto-electronic applications. Many efforts have been made to produce a material to overcome this difficulty. The group-III nitrides are currently being actively investigated in view of their promising potential for short-wavelength electroluminescence devices and high-temperature, high-power, and high-frequency electronics. These semiconductors have received considerable attention both experimentally [1–8] and theoretically [9–13]. A number of reviews on GaN and AlN were given by Strite and Morkoc [14], Davis et al.[15], and Pankove [16]. The vast majority of research on III–V nitrides has been focused on the wurtzite crystal phase. The reason is that most of III–V nitrides have grown on sapphire substrates which generally transfer their hexagonal symmetry to the nitride film. Under high pressure these nitride compounds undergo a structural phase transformations to the rocksalt structure which is favored by high ionicity [17,18]. However, there has been less work on $Al_{0.5}In_{0.5}N$ alloy, and little information on its band-structure exists.

The annihilation of positrons in solids has been found to be a useful probe for obtaining information about the momentum distribution of the electrons [19]. This method became an important tool for the investigation of the electronic structure of metals and for understanding the behavior of electrons in crystals. However, to understand the results of positron annihilation, it is necessary to have an insight about how positron will annihilate in semiconductors by means of electron and positron distributions for two different kinds of semiconductors.

The investigation of electronic properties of solids using electronic and positron charge densities represent an increasing importance. So far, this work has been concerned with electronic charge densities, which were

*Corresponding author.
E-mail address: babbar@univ-sba.dz (B. Abbar).

0022-4596/$ - see front matter © 2005 Elsevier Inc. All rights reserved.
doi:10.1016/j.jssc.2005.03.047

found to be useful for understanding the chemical bonds and the modification of the band structures by in interstitial impurities [20,21]. Positron charge densities provided complementary information, they have been used quite extensively in a variety of materials [22,23]. The great success of the recent development in this field motivated us to look for a better understanding of the charge densities.

So far, the group-III nitrides and their alloys are relatively less studied and few calculations have been reported on their charge densities [24,25]. This has prompted us to take such a calculation in zinc-blende III–V semiconductors, particularly $Al_{1-x}In_xN$ alloy. The aim of this work is to prospect the future of positronic and electronic charge densities on zinc-blende AlN, InN and their alloy $Al_{0.5}In_{0.5}N$.The calculations of the present work are based the density-functional theory [26] in the generalized gradient approximation (GGA) for exchange and correlation. First, the self-consistent electron structures are calculated by the full potential linearized augmented plane wave (FP-LAPW) method [27]. Thereafter, the positron potential is determined within GGA for the electron–positron correlation effects, and the positron wave function and energy eigenvalue are calculated also using the same method.

2. Method of calculation

Self-consistent calculations of total energies and the electronic structure based on the non-scalar relatisvitic full-potential (FP) "linearized augmented plane wave + local orbitals"(LAPW + lo) method were carried out using the WIEN2k code [27]. This is very accurate and efficient scheme to solve the Kohn–Sham equations of density functional theory (DFT) in which exchange and correlation effects are treated, for example, by the GGA [26] which often leads to better energetics and equilibrium structures than the local density approximation (LDA) [28]. The electron density is obtained by summing over all occupied Kohn–Sham orbitals and plays the key role in the formalism. The atomic sphere radii were 1.7 bohr for Al, 1.9 bohr for In and 1.6 bohr for N. The required precision in total energy was achieved by using a large plane wave (PW) cutoff. In the linear APW (LAPW) method the relevant convergence parameter is R_{MT}. k_{max}, which is defined by the product of the smallest atomic sphere radius times the largest reciprocal lattice vector of the PW basis. We use R_{MT}. $k_{max} = 9$ for AlN and InN and ternary alloy. This corresponds to an energy cutoff of 14 Ry.

The binaries compounds crystallize in the zinc-blende structure AC,BC ($F\bar{4}3m$), the disordered ternary alloy at 50% is modelled using a supercell with 8 atoms in the (P) structure. The k integration over the Brillouin zone is performed using the Monkhorst and Pack mesh [29]. A mesh of 30 special k-points was taken in the irreducible wedge of the Brillouin zone for the binary cases and for the ternary alloy. The iteration process was repeated until the calculated total energy of the crystal converge to less than 1 mRyd. A total of 7 iterations were necessary to achieve self-consistency. We compute lattice constants, bulk moduli and their first derivatives by fitting the total energy versus volume according to the Murnaghan's equation of state [30].

The foundation for modern electronic structure calculations for solids is the density-functional theory based on the work by Hohenberg and Kohn [31] and by Kohn and Sham [32]. During the last two decades, the ab initio electronic-structure-calculation methods developed rapidly, and nowadays most of the important basic properties of solids, such as the structural and cohesive properties, can be calculated without any adjustment to the experimental results [33]. In this article, we are interested in how to determine electron and positron states in solids and how to determine electron and positron energy levels and their charge densities. It turn out that the ab initio determination of positron states in solids is possible on the basis of the two-component generalization of the density-functional theory [34–37].

In two-component density-functional theory, the ground-state energy of system of electron and positron in an external V_{ext} is written as a function of the electron (n_-) and positron (n_+) densities [37]

$$E[n_-,n_+] = F[n_-] + F[n_+] + \int d\mathbf{r}\mathbf{V}_{ext}(\mathbf{r})[n_-(\mathbf{r}) - n_+(\mathbf{r})] - \int d\mathbf{r}\int d\mathbf{r}'\frac{n_-(\mathbf{r})n_+(\mathbf{r}')}{|\mathbf{r}-\mathbf{r}'|} + E_c^{e-p}[n_+,n_-], \quad (1)$$

where $F(n)$ denotes the following one-component functional for electrons or positrons

$$F[n] = T[n] + \frac{1}{2}\int d\mathbf{r}\int d\mathbf{r}'\frac{n(\mathbf{r})n(\mathbf{r}')}{|\mathbf{r}-\mathbf{r}'|} + E_{xc}[n]. \quad (2)$$

$T(n)$ is the kinetic energy of non-interacting electrons or positrons, and $E_{xc}[n]$ is the exchange-correlation energy between indistinguishable particles. Finally, $E_c^{e-p}[n_+,n_-]$ in Eq. (1) is the electron–positron correlation-energy functional.

The ground-state electron and positron densities minimizing $E[n_-,n_+]$ can be calculated using a generalized Kohn–Sham method, which requires the solving of the following set of one-particle Schrödinger equations for electrons and positrons

$$-\frac{1}{2}\nabla^2\psi_i(r) + \left[\frac{\delta E_{xc}[n_-]}{\delta n_-(r)} - \phi(\mathbf{r}) + \frac{\delta E_c^{e-p}[n_+,n_-]}{\delta n_-(\mathbf{r})}\right] \psi_i(\mathbf{r}) = \varepsilon_i\psi_i(\mathbf{r}), \quad (3)$$

$$-\frac{1}{2}\nabla^2\psi_i^+(r)+\left[\frac{\delta E_{xc}[n_+]}{\delta n_+(r)}+\phi(r)+\frac{\delta E_c^{e-p}[n_+,n_-]}{\delta n_+(r)}\right]$$
$$\psi_i^+(r)=\varepsilon_i^+\psi_i^+(r), \quad (4)$$

where

$$\phi(\mathbf{r})=\int d\mathbf{r}'\,\frac{-n_-(\mathbf{r}')+n_+(\mathbf{r}')+n_0(\mathbf{r}')}{|\mathbf{r}-\mathbf{r}'|} \quad (5)$$

is the total Coulomb potential and $n_0(\mathbf{r})$ denotes the (positive) charge density providing the external potential V_{ext}. The electron and positron densities are calculated by summing over the occupied states (ε_F is the electron energy Fermi and N_+ is the number of positrons)

$$n_-(r)=\sum_{\varepsilon_i\leqslant\varepsilon_F}\left|\psi_i(\mathbf{r})\right|^2,$$
$$n_+(r)=\sum_{i}^{N_+}\left|\psi_i^+(\mathbf{r})\right|^2. \quad (6)$$

Eqs. (3)–(5) have to be solved self-consistently and simultaneously for electron and positron states, using an iterative scheme.

The above method [Eqs. (1)–(6)] would be exact if the exchange-correlation energy functional $E_{xc}[n]$ and the electron–positron correlation-energy functional $E_c^{e-p}[n_+,n_-]$ were known. Unfortunately, this is not the case. In electronic structure calculations the most popular way to continue is to make the LDA for exchange-correlation effects. Local-density approximation means that the exchange-correlation energy is approximated as

$$E_{xc}[n]=\int n(\mathbf{r})\varepsilon_{xc}(n(\mathbf{r})\,d\mathbf{r}, \quad (7)$$

where $\varepsilon_{xc}(n)$ is the exchange-correlation energy per particle in a homogeneous one-component gas. In Eqs. (3) and (4), the functional derivatives of $E_{xc}[n]$ becomes a function of density. This function is called the exchange-correlation potential

$$\mu_{xc}(n)=\frac{\delta E_{xc}[n]}{\delta n(r)}=\frac{\delta[n\varepsilon_{xc}(n)]}{\delta n}. \quad (8)$$

The exchange-correlation energy $\varepsilon_{xc}(n)$ for a homogeneous electron gas is well known from the quantum Monte Carlo simulations by Ceperley and Alder [38]. (Practical parametrizations of their local exchange-correlation functional are given, for example, by Perdew and Zunger [39] and by Perdew and Wang [28].)

For a delocalized positron in a perfect crystal lattice, the two-component density theory simplifies essentially. Because the positron density in this case is vanishingly small at every point of the (infinite) lattice, it cannot influence the electronic structure. The electronic structure of the perfect lattice is therefore first solved by some standard self-consistent band structure code. This code solves the Kohn–Sham equations obtained from Eqs. (3), (5), and (6) by omitting the positron n_+ and the electron–positron correlation potential $\delta E_c^{e-p}[n_+,n_-]/\delta n_-(r)$. For example, the effective electron potential is

$$v_{eff}(r)=-\phi(r)+v_{xc}(n_-(r)), \quad (9)$$

where $\phi(\mathbf{r})$is the Coulomb potential due the nuclei and electron charge density and v_{xc} is the GGA [26] exchange-correlation, which depends on the electron density $n_-(\mathbf{r})$.

The potential sensed by the positron is constructed as the sum of the Coulomb potential ϕ (from the electronic structure calculation) and the correlation potential V_{corr},

$$V_+(\mathbf{r})=\phi(\mathbf{r})+V_{corr}(n_-(\mathbf{r})). \quad (10)$$

The correlation potential V_{corr} is the zero-positron-density limit of the electron–positron correlation potential $\delta E_c^{e-p}[n_+,n_-]/\delta n_+(\mathbf{r})$. V_{corr} is equal to the (correlation) energy for a delocalized positron in a homogeneous electron gas [40].

3. Results and discussions

Fig. (1) displays the crystal structure of the alloy $Al_{0.5}In_{0.5}N$. In Table 1 we compare the calculated data with experiment and with results obtained from previous calculations. The LDA values are smaller than the experiment data (i.e., smaller lattices). By contrast, our GGA are slightly larger (by 0.45–1.2%) compared to the experimental lattice sizes. The LDA generally overestimates bulk moduli. The values obtained in our work are in agreement with the results of first-principles full potential linear muffin-tin orbital calculations [41] to within a few percent.

To provide a basis for understanding future energy gap device concepts and application based on zinc-blende III–V nitrides semiconductors, we have computed the electronic band structure of zinc-blende

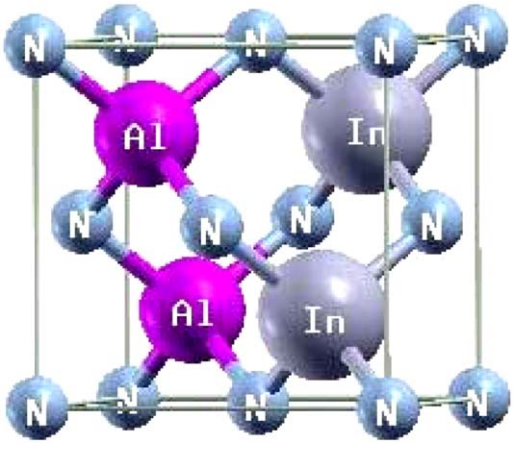

Fig. 1. Crystal structure of zinc-blende $Al_{0.5}In_{0.5}N$.

Table 1
Equilibrium lattice constants, bulk moduli and their derivatives of zinc-blende AlN, InN and $Al_{0.5}In_{0.5}N$ Other theoretical and experimental data are in parentheses

	AlN	InN	$Al_{0.5}In_{0.5}N$
Present work LDA			
V (Å)	37.05	30.22	102.79
a (Å)	4.35, (4.32[a]),(4.38[b])	4.94, (4.46[a]), (4.98[c])	4.68
B	209(203[a])	146(139[a])	175
B'	3.89(3.2[a])	4.48(4.4[a])	4.64
E_0	−592.84	−11865.07	−24915,66
Present work GGA			
V (Å)	21.39	32.15	108.58
a (Å)	4.40	5.04	4.77
B	192	133	153
B'	3.76	3.36	4.83
E_0	−595.36	−11876.12	−24942.80

[a]From Ref. [41].
[b]From Ref. [42].
[c]From Ref. [43].

Table 2
Zinc-blende AlN and InN energies in eV at high symmetry-points in LDA [24] (GGA). All values refer to the top of the valence band.

High symmetry-points	AlN	InN
Γ_1^v	−14.47(−14.85)	−13.53(−13.49)
Γ_{15}^v	0.00(0.00)	0.00(0.00)
Γ_1^c	3.66(3.94)	0.00(0.00)
Γ_{15}^c	11.72(12.28)	9.33(9.17)
X_1^v	−11.93(−12.26)	−10.87(−11.06)
X_5^v	−1.73(−1.77)	−2.43(−2.19)
X_1^c	3.21(3.30)	2.81(2.88)
X_3^c	8.03(8.45)	5.93(5.68)
L_1^c	6.69(7.12)	3.07(2.91)
L_1^v	−12.53(−12.87)	−11.26(−11.42)
L_3^v	−0.48(−0.49)	−0.90(−0.82)
L_3^c	9.34(7.12)	6.49(6.39)

$Al_{1-x}In_xN$ alloys. The energies calculated using the FP-LAPW method for zinc-blende AlN, InN are listed in Table 2 for the high-symmetry points Γ, X and L in the Brillouin zone.

All energies are with reference to the top of the valence band Γ_{15}^v. The band structures of AlN, InN and $Al_{0.5}In_{0.5}N$ are shown in Figs. 2–4, respectively. The results show that InN is a direct-gap semiconductor with the minimum of conduction band at Γ point. We know that AlN the wurtzite structure whose electronic structure was fully studied a few years ago [24,25,44,45]. A feature worth noting with regard to zinc-blende AlN, is that it has an indirect minimum energy gap (at X point) in contrast to the direct gap observed in wurtzite AlN. Zinc-blende $Al_{1-x}In_xN$ alloys should, therefore, have an indirect gap for small values

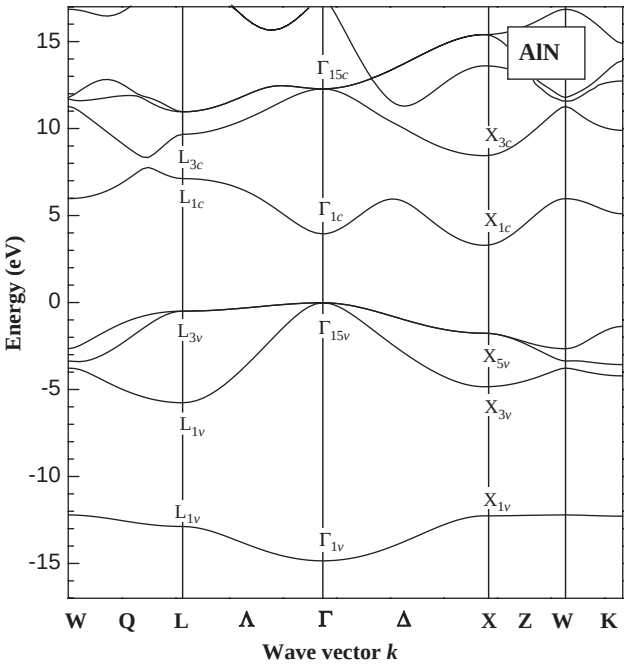

Fig. 2. Electronic band structures of zinc-blende AlN.

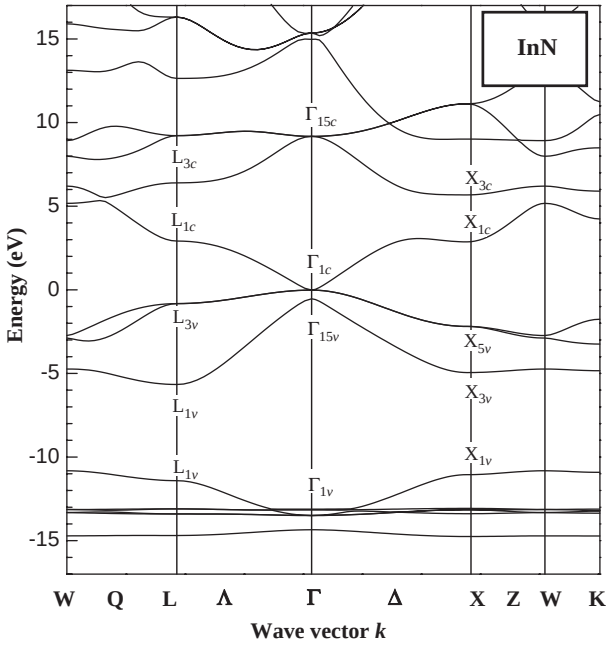

Fig. 3. Electronic band structures of zinc-blende InN.

of x and a direct gap for large values. It is found that there is a good agreement between our results and other work [46]. The calculated energy gaps of AlN E_g^X and InN E_g^Γ are 3.20 and 0.00 eV, respectively, which are in good agreement with the theoretical values [47,48] as listed in Table 3. The experimental measured energy gap of zinc-blende InN E_g^Γ is 1.9 eV [49]. In comparison, the

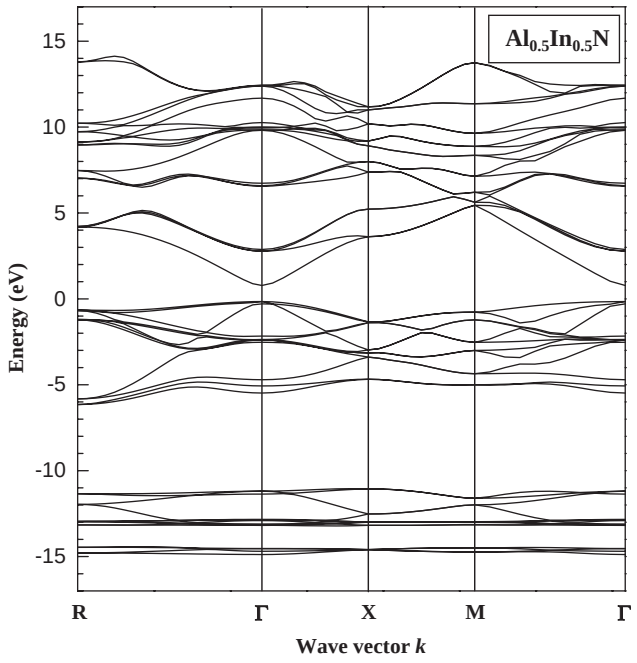

Fig. 4. Electronic band structures of zinc-blende $Al_{0.5}In_{0.5}N$.

Table 3
The energy bands in eV of zinc-blende AlN, InN and $Al_{0.5}In_{0.5}N$. Other theoretical and experimental data are given in parentheses

Energy gap	AlN	InN	$Al_{0.5}In_{0.5}N$
Our LDA work			
E_g^{Γ}	3.66 (6[a]) (4.1[d])	0(–0.09[b])(1.9[c]) (0.4[d])	0.93
E_g^{X}	3.21 (4.9[a]) (3.2[d])	2.80 (2.85[b]) (2.8[d])	3.77
$E_g^{L,M}$	6.68 (9.3[a])	3.07 (3.37[b])	5.61
Antisymmetric gap	7.16	5.62	
Our GGA work			
E_g^{Γ}	3.92	0	1.18
E_g^{X}	3.28	2.87	3.87
$E_g^{L,M}$	7.10	2.91	5.81
Antisymmetric gap	7.42	6.01	

[a]Quasiparticle results from Ref. [12].
[b]Theoretical results from Ref. [47].
[c]Experimental results from Ref. [49].
[d]LDA calculations from Ref. [48].

LDA underestimates the energy band gap. As yet, in the literature, there is a lack of zinc-blende $Al_{0.5}In_{0.5}N$ experimental data regarding the band structures and to our knowledge no theoretical reports have been carried out by other authors for a direct comparison.

The calculated band gap exhibits strong composition dependence. The strongest contribution to the gap is due may be to a structural effect i.e. The composition-induced disorder in the bond lengths. This is different from conventional III–V alloys which show a weakly composition-dependent band gap [50,51]. The fundamental gap for $Al_{1-x}In_xN$ ranges from 3.92 eV ($x = 0$) to 1.18 eV ($x = 0.5$) to 0 eV ($x = 1$). The extraction of the gap bowing parameter of AlInN from various optical measurements requires knowledge of the band gaps of the binary compounds AlN and InN. While the band gap is well known today, the band structure of InN is rather uncertain, because of sample-quality problems. Results found by Yamaguchi et al. [52], who measured the peak position of the PL at about 1.66 eV for $Al_{1-x}In_xN$ alloys for $x = 0.6$. Optical absorption and photoluminescence measurements of high-quality samples, as a well as quasiparticle calculations beyond DFT-LDA, seem to tend to InN energy gaps close to 1 eV [53]. More reliable experimental studies are highly desirable, since a lower value of the band gap of InN will dramatically reduce the difference between bowing parameters determined experimentally or theoretically. First principles calculations have been performed for ordered and disordered zinc-blende $Al_{0.5}In_{0.5}N$ alloys including full relaxation of bond lengths and bond angles [46]. The formation enthalpies for the disordered and ordered (CuAu and chalcopyrite) alloys are given by Wright et al. [46] for both unrelaxed and fully relaxed structures. The unrelaxed formation enthalpies are large ($\approx +0.24$ eV/atom) which is expected given the strong bonds in these compounds and their 12.7% lattice mismatch. The relaxed formation enthalpies for disordered alloys are within 3 meV/atom of each other. To the extent that these structures approximate a disordered alloy, this indicates that their formation enthalpies provide reasonable estimates of the $Al_{0.5}In_{0.5}N$ mixing enthalpy. In addition, we note that the chalcopyrite formation enthalpy is lower than the mixing enthalpy whereas the CuAu formation enthalpy is higher. This consistent with results for other III–V semiconductor

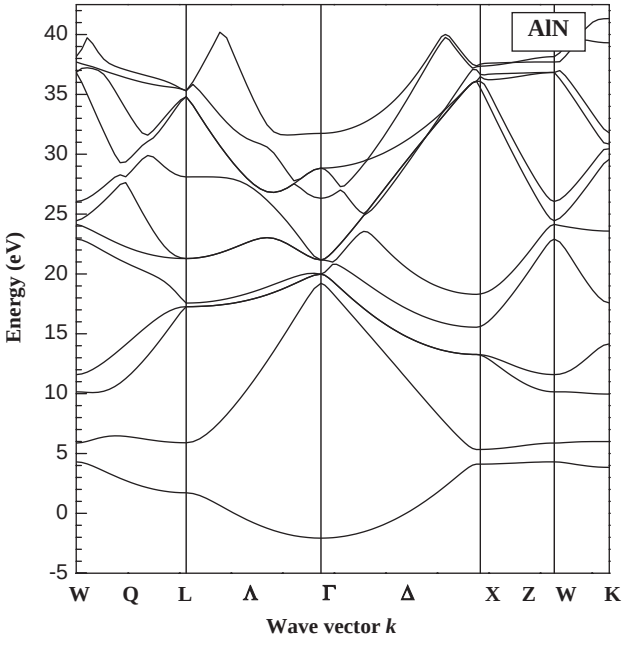

Fig. 5. Positronic band structures of zinc-blende AlN.

alloys [54]. As shown in Table 3 the value of the antisymmetric gap is larger in AlN than InN. Since this gap is related to the ionicity of the semiconductors [55], we obtain that AlN is slightly more ionic material than InN.

The positron band structures for AlN, InN and $Al_{0.5}In_{0.5}N$ are displayed in Figs. 5–7, respectively. The first obvious observation is the similarity between the positron and electron energy spectrum, with the exception that the positron energy spectrum does not exhibit a band gap. The lowest positron energy state is the Γ state at $k_+ = 0$.

To visualize the nature of the bond character and to explain the charge transfer and the bonding properties of AlN, InN and their alloy $Al_{0.5}In_{0.5}N$, we calculate the total valence charge density. We show in Figs. 8–10 the total valence charge densities along the $\langle 111 \rangle$ direction and the (110) plane for each material. The calculated electron charge distribution indicates that there is a strong ionic character as can be seen along the Al–N and In–N bonds. The nitrogen ions are larger than the aluminum (indium) ions for both cases. The driving force behind the displacement of the bonding charge is the greater ability of N to attract electrons towards it due to the difference in the electronegativity of Al and N and of In and N ($\chi_N - \chi_{Al} = 1.43, \chi_N - \chi_{In} = 1.26$). Because of the large mixing of the wave functions for $Al_{0.5}In_{0.5}N$, this alloy has a charge density whose

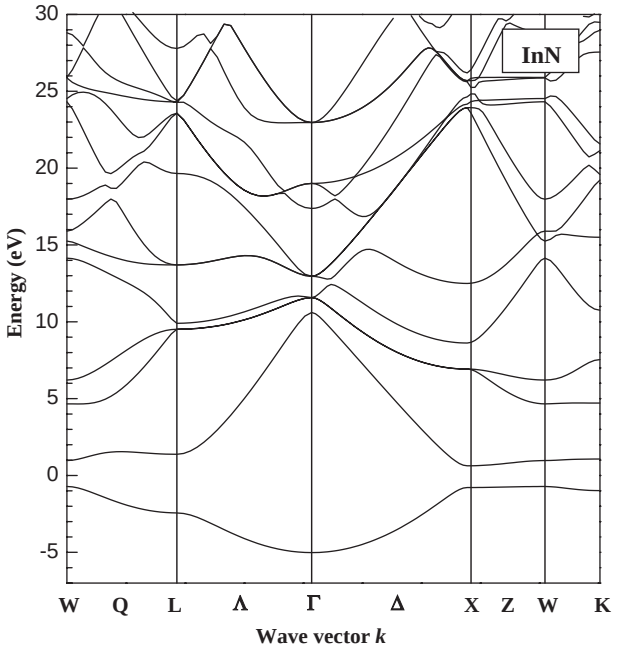

Fig. 6. Positronic band structures of zinc-blende InN.

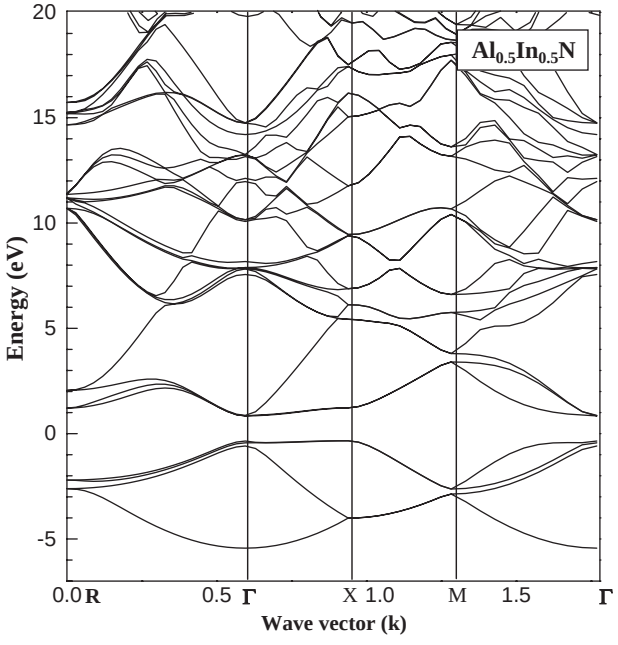

Fig. 7. Positronic band structures of zinc-blende $Al_{0.5}In_{0.5}N$.

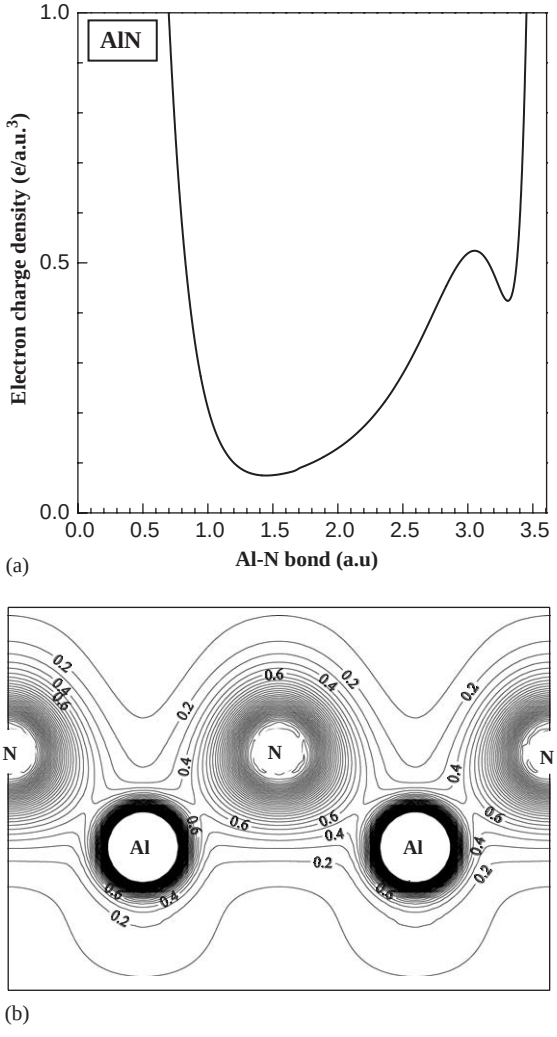

Fig. 8. Total valence charge densities in zinc-blende AlN (a) along the $\langle 111 \rangle$ direction, (b) in the (110) plane.

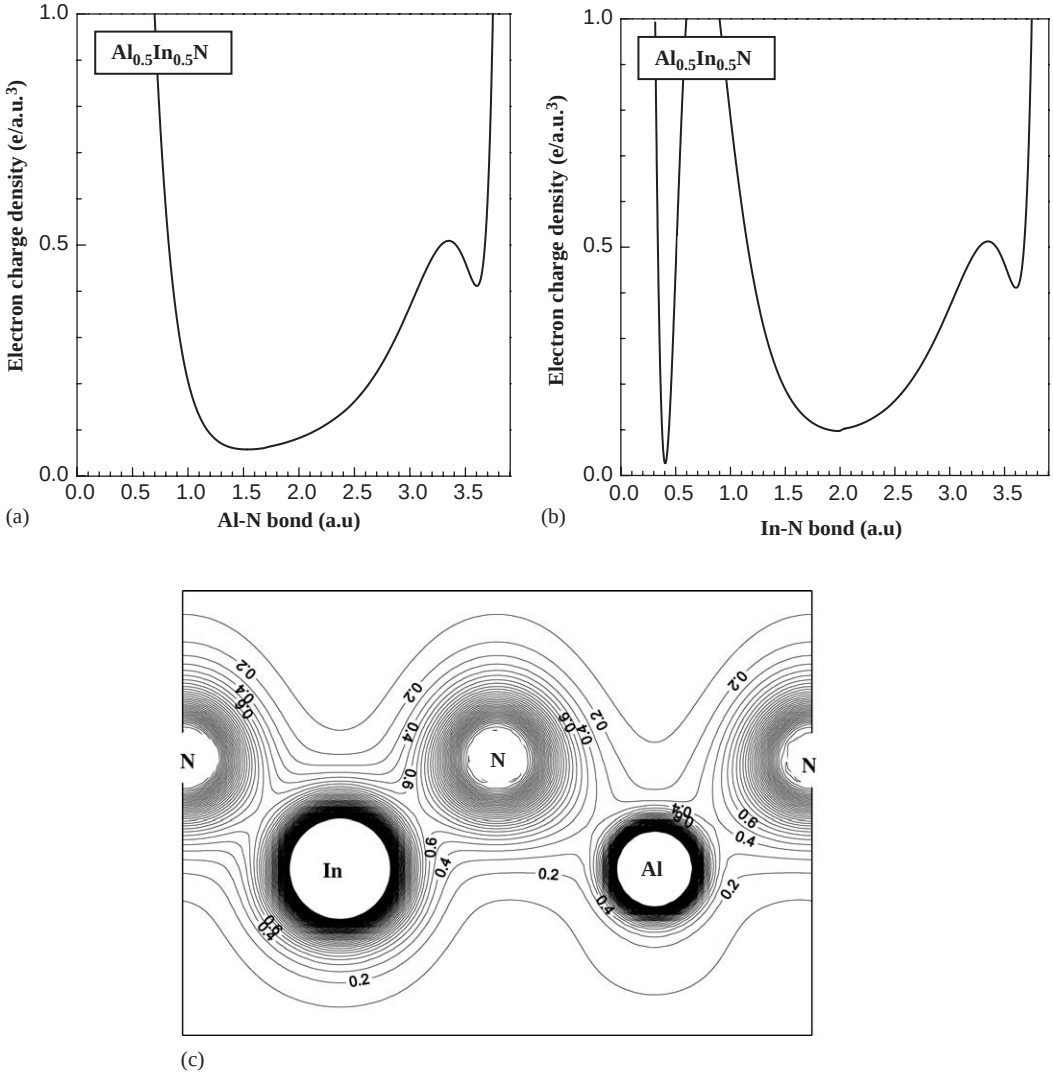

Fig. 9. Total valence charge densities in zinc-blende $Al_{0.5}In_{0.5}N$ (a) along the Al–N bond direction, (b) along the In–N bond direction, (c) in the (110) plane.

characteristic is intermediate between those of AlN and InN.

Three different approaches have been used to calculate the ionicity factor for AlN and InN binary compounds: (i) the model of Zaoui et al. based on the valence charge density calculations [56], (ii) the Pauling definition based on the electronegativity values of the elements [57] and the Garcia–Cohen approach based on the valence charge density calculation [18].

The Zaoui et al. ionicity factor is defined as [56]

$$f_i = \left(\frac{S_A}{S_A + \lambda S_C}\right)^{\lambda}, \tag{11}$$

where S_A is the area of the anion charge density, S_C the area of the cation charge density and $\lambda = -1$ for the compounds IV–IV and III–V.

We also use the Pauling definition [57] of the ionicity of a single bond and the Philips electronegativity values for N and Al; a rapid estimation of the ionicity factor is obtained by using the Pauling equation:

$$f_i^P = 1 - \exp[-[\chi_A - \chi_B]^2/4], \tag{12}$$

where χ_A and χ_B are the electronegativities of atoms A and B, respectively.

The scaling law by Garcia and Cohen was successfully in predicting the f_i behavior for a wide variety of semiconductors. However, these authors calculated the charge densities using the total-energy pseudopotential method, and the deduced ionicity factors exhibited a large discrepancy with the Phillips ionicity scale for all the group-III nitrides. The Garcia–Cohen ionicity factor is defined as

$$f_i = \sqrt{S_s/S_a}, \tag{13}$$

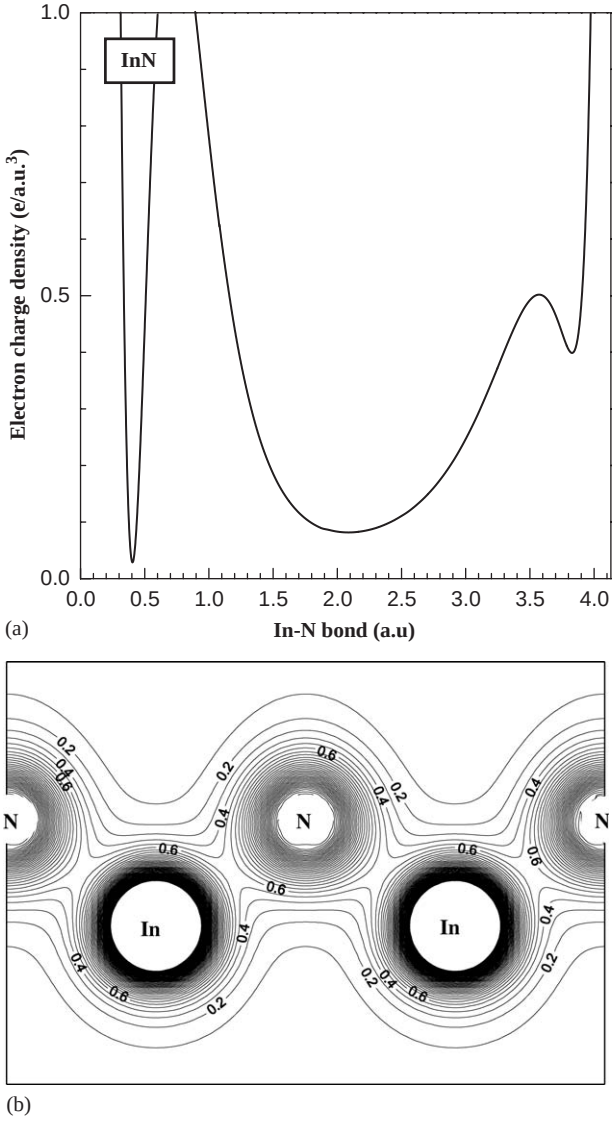

Fig. 10. Total valence charge densities in zinc-blende InN (a) along the $\langle 111 \rangle$ direction, (b) in the (110) plane.

where S_s and S_a are the measures of the strength of the symmetric and antisymmetric components of the charge density, respectively, and are defined as [18]

$$S_{s/a} = (1/V_0) \int_{V_0} \rho^2_{s/a} d^3r. \quad (14)$$

The calculated ionicity values for AlN and InN are given in Table 4. We notice that the value of f_i for a same compound is different following the used method of calculations. The calculated values of 0.53 for AlN and 0.46 for InN are close to those given by Phillips [17] but are very different to that found by Garcia and Cohen [18].

Using the model potential and basis set described in the previous section, we computed the positron charge density at the bottom of the lowest band for each material. These charge densities are calculated along the normal nearest-neighbor tetrahedral distance (the $\langle 111 \rangle$ axis) and in the (110) plane.

Positron charge densities for AlN, $Al_{0.5}In_{0.5}N$ and InN, respectively, are displayed in Figs. 11–13. The first

Table 4
The calculated ionicity factor f_i of AlN and InN.

Materials	f_i
AlN	0.40[a] 0.75[b] 0.53[c]
InN	0.32[a] 0.62[b] 0.46[c]

[a]Estimated using the Pauling definition [57].
[b]Calculated using the model of Zaoui et al. [56].
[c]Estimated using Garcia–Cohen approach [18].

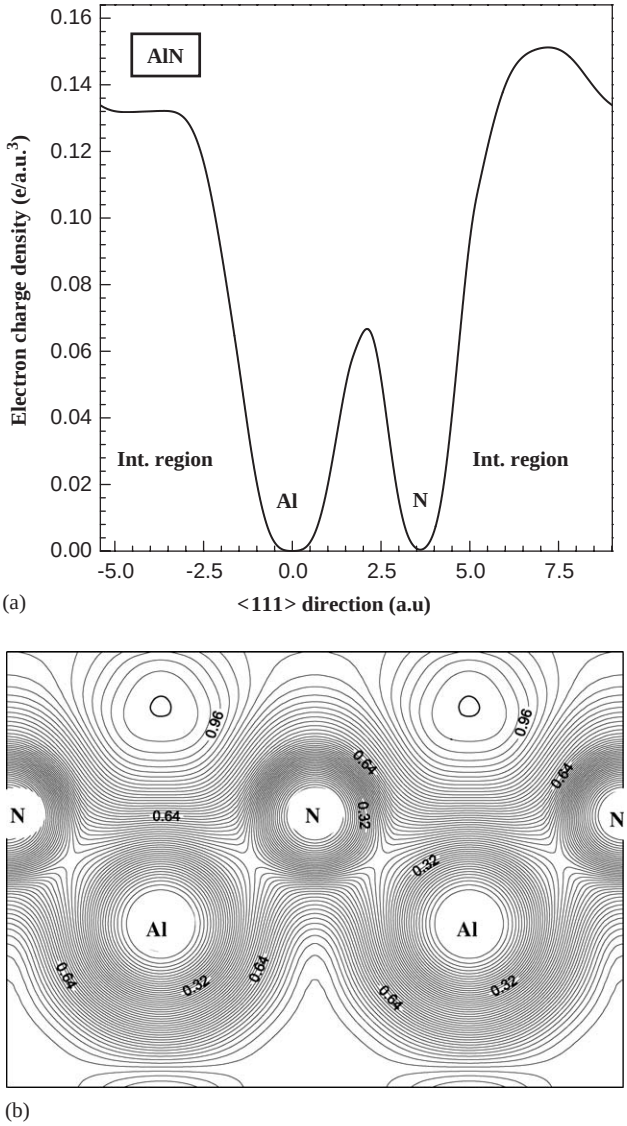

Fig. 11. Positronic charge densities at point Γ in zinc-blende AlN (a) along the $\langle 111 \rangle$ direction, (b) in the (110) plane.

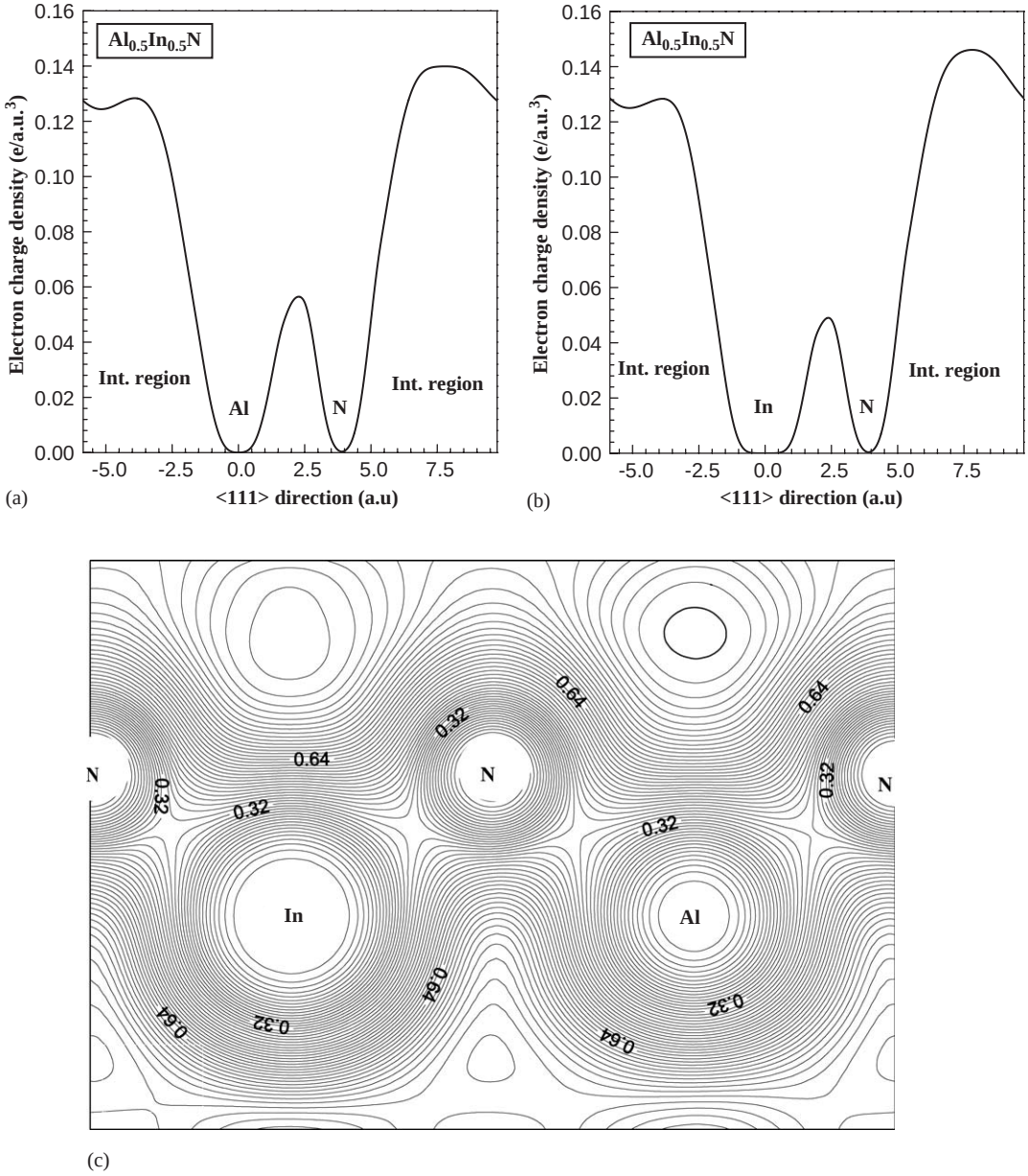

Fig. 12. Positronic charge densities at point Γ in zinc-blende $Al_{0.5}In_{0.5}N$ (a) along the Al–N bond direction, (b) along the In–N bond direction, (c) in the (110) plane.

observation is that there a large charge density between atoms. Contrary to previous works performed so far [58], the calculations carried out here taking valence and core electrons into account are based on first-principles method. At the bond center the magnitude is smaller for InN than for AlN, because in InN the positron density concentrates strongly into the interstitial regions, decreasing the core electrons effect. The system presented, being able to predict quantities such as S and W line-shape parameters [59] directly measurable by slow-positron-beam techniques, is a useful tool to be employed as a support to the experiments concerning various kinds of problems of bulk solids.

Qualitatively, these charge densities present nearly the same characteristics, since there is a clear asymmetrical positron charge distribution relative to the bond center. Furthermore, it is clear that the positron is located in the interstitial region and between atoms and that the positron density is reduced almost to vanishing point in the immediate vicinity of the ion cores. At no point along the nearest neighbor Al–N (In–N) vector is the positron density more than 40% of its peak in the interstitial regions. The maximum point of the probability is found to be located at the tetrahedral site and between atoms. From the quantitative point of view, there is a difference of charge in the interstitial regions.

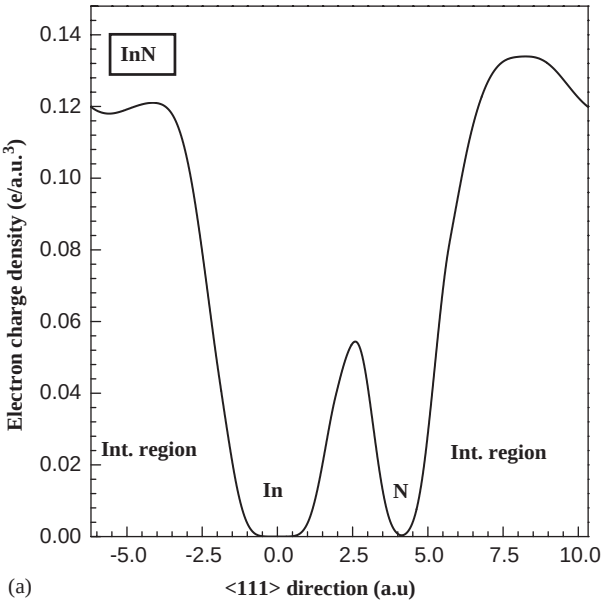

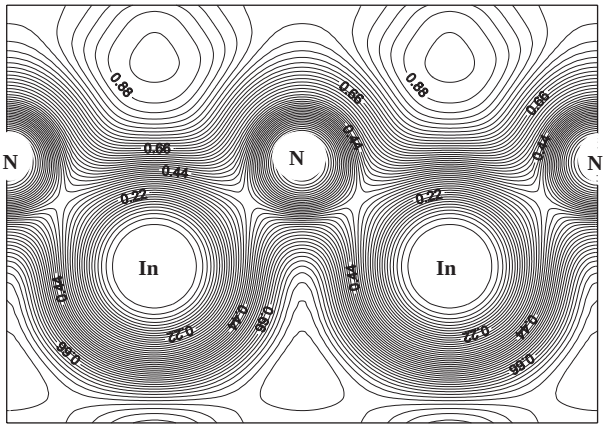

Fig. 13. Positronic charge densities at point Γ in zinc-blende InN (a) along the $\langle 111 \rangle$ direction, (b) in the (110) plane.

Table 5
Relevant charge densities at different positions in AlN, $Al_{0.5}In_{0.5}N$, InN

Material	C. int	Bond center	A. int
AlN	0.132	0.067	0.151
$Al_{0.5}In_{0.5}N$			
Al–N	0.128	0.056	0.139
In–N	0.128	0.049	0.146
InN	0.121	0.054	0.134

C. int: cation interstitial region.
A. int: anion interstitial region in the same arbitrary units.

The positron distribution is more pronounced in the neighborhood of the N anion than that in that of the Al(In) cation. The corresponding charge densities for different positions are listed in Table 5. At the cation interstitial region, when we go from one binary semiconductor, AlN, to another one, InN, through the ternary alloy $Al_{0.5}In_{0.5}N$, a fluctuation in the positron charge density is seen which reaches a maximum value due to the effect of Al, whereas an decrease in the positron charge density corresponds to the dominance of In. At the bond center the situation is quite different, since the positron charge density also decreases. This suggests that the positron tends to fill the inter-nuclear spacing, which could be explained as charge transfer from the cation interstitial region to that of the anion. We find that the same effect occurs at the anion interstitial region but is larger. We may conclude that there is a strong affinity of positrons for the anion. Ultimately, these results will lead us to think that the positron may preferentially annihilate with anion rather than the cation. This work reveals several possibilities for the study of positron annihilation in ternary alloys.

4. Conclusion

We have presented a study of the electronic and positronic band structures of AlN, InN and $Al_{0.5}In_{0.5}N$. The electronic band structures from the FP-LAPW calculations are attested by a comparison with experimental data and theoretical results. InN and $Al_{0.5}In_{0.5}N$ resulted as direct while zinc-blende AlN resulted as indirect semiconductor from our calculations. We showed critical point transition energies for AlN and InN, which could be useful for future experimental studies of these materials. We provided information about the electron charge densities, which allows us to evaluate the charge transfer in the two binary compounds. The ionicity factors also were calculated with three approaches. The calculated results of the positron charge density reflected the high insight for the annihilation effect. The positrons are repelled by the positively charged atomic cores and tend to move in the interstitial regions. The system presented, being able to predict quantities such as S and W line-shape parameters directly measurable by slow-positron-beam techniques, is a useful tool to be employed as a support to the experiments concerning various kinds of problems of bulk solids. Further work on positron annihilation in binary compounds and ternary alloys is under progress.

References

[1] W.C. Johnson, J.B. Parsons, M.C. Crew, J. Phys. Chem. 36 (1982) 2561.
[2] E. Tiede, M. Thimann, K. Sensse, Chem. Berichte 61 (1928) 1568.
[3] H.P. Maruska, J.J. Tieten, Appl. Phys. Lett. 15 (1969) 327.
[4] Trieste (Ed.), Proceedings of the 7th ICTP-IUAP Semiconductor Symposium, in: C.G. van de Walle, Physica 185B (1993) R9.

[5] T. Lei, T.D. Moustakas, R.J. Graham, Y. He, S.J. Berhowitz, J. Appl. Phys. 71 (1992) 4933.
[6] T. Lei, M. Fanciulli, R.J. Molnar, T.D. Moustakas, R.J. Graham, J. Scanlon, Appl. Phys. Lett. 95 (1991) 944.
[7] M.J. Paisley, Z. Sitar, J.B. Posthill, R.F. Davis, J. Vac. Sci. Technol. A 7 (1989) 701.
[8] Z. Sitar, M.J. Paisley, J. Rnan, J.W. Choyke, R.F. Davis, J. Mater. Sci. Lett. 11 (1992) 261.
[9] S. Bloom, G. Harbeke, E. Meier, I.B. Ortenburger, Phys. Stat. Sol. (B) 66 (1974) 161.
[10] P.E. van Camp, V.E. van Doren, J.T. Devresse, Phys. Rev. B 44 (1991) 9056.
[11] A. Munoz, K. Kune, Phys. Rev. B 44 (1991) 10372.
[12] A. Rubio, J.L. Corkill, M.L. Corkill, M.L. Cohen, E.L. Shirley, S.G. Louie, Phys. Rev. B 48 (1993) 11810.
[13] A.F. Wright, J.S. Nelson, Phys. Rev. B 50 (1994) 2159.
[14] S. Strite, H. Morkoc, J. Vac. Sci. Technol. B 10 (1992) 1237.
[15] R.F. Davis, Z. Sitar, B.E. Williams, H.S. Kong, H.J. Kim, J.W. Palmour, J.A. Edmond, J. Ryu, J.T. Glas, C.H. Carter Jr, Mater. Sci. Eng. B 1 (1988) 77.
[16] J.I. Pankove, Mater. Res. Soc. Symp. Proc. 97 (1987) 409; J.I. Pankove, Mater. Res. Soc. Symp. Proc. 162 (1990) 515.
[17] J.C. Philips, Rev. Mod. Phys. 42 (1970) 317.
[18] A. Garcia, M.L. Cohen, Phys. Rev. B 47 (1993) 4215.
[19] H. Aourag, A. Belaidi, T. Kobayashi, R.N. West, B. Khelifa, Phys. Stat. Sol. B 156 (1989) 497.
[20] S.L. Richardson, M.L. Cohen, Phys. Rev. B 35 (1987) 1388.
[21] H. Aourag, B. Khelifa, A. Belaidi, L. Hamerlaine, H. Belarbi, Phys. Lett. A 145 (1990) 455.
[22] H. Aourag, A. Belaidi, T. Kobayasi, R.N. West, B. Khelifa, Phys. Stat. Sol. (B) 156 (1989) 497.
[23] H. Aourag, B. Khelifa, A. Belaidi, Z. Belarbi, Phys. Stat. Sol. (B) 160 (1990) 201.
[24] V.I. Nefedov, Structure of Molecules and Chemical Bonding, Volume 3: Valence electronic levels of chemical compounds (according to photoelectronic, electronic and X-ray spectroscopies). Moscou: VNIITI, 172, 1975.
[25] Y.N. Xu, W.-Y. Ching, Electronic optical and structural properties of some wurtzite crystals, Phys. Rev. B 48-1(7) (1993) 4335–4351.
[26] J.P. Perdew, S. Burke, M. Ernzerhof, Phys. Rev. Lett. 77 (1996) 3865.
[27] P. Blaha, K. Schwarz, G.K.H. Madsen, D. Kvasnicka, J. Luitz, WIEN2k, An Augmented Plane Wave Plus Local Orbitals Program for Calculating Crystal Properties, Vienna University of Technology, Vienna, Austria, 2001.
[28] J.P. Perdew, Y. Wang, Phys. Rev. B 45 (1992) 13244.
[29] H.J. Monkhorst, J.D. Pack, Phys. Rev. 13 (1976) 5188.
[30] F.D. Murnaghan, Proc. Natl. Acad. Sci. USA 30 (1944) 5390.
[31] P- Hohenberg, W. Kohn, Phys. Rev. 136 (1964) B864.
[32] W. Kohn, L.J. Sham, Phys. Rev. 140 (1965) A1133.
[33] R.O. Jones, O. Gunnarson, Rev. Mod. Phys. 61 (1989) 689.
[34] B. Chakraborty, R.W. Siegel, Phys. Rev. B 27 (1983) 4535.
[35] S. Lundqvist, N.H. March (Eds.), Theory of the Inhomogeneous Electron Gas, Plenium, New York, 1983.
[36] R.M. Nieminen, E. Boronski, L. Lantto, Phys. Rev. B 32 (1985) 1377.
[37] E. Boronski, R.M. Nieminen, Phys. Rev. B 34 (1986) 3820.
[38] D.M. Ceperley, B.J. Alder, Phys. Rev. Lett. 45 (1980) 566.
[39] J.P. Perdew, A. Zunger, Phys. Rev. B 23 (1981) 5048.
[40] M.J. Puska, R.M. Nieminen, Rev. Mod. Phys. 66 (3) (1994).
[41] K. Kim, W.R. Lambrecht, B. Segall, Phys. Rev. B 53 (1996) 16310.
[42] I. Petrov, E. Mojab, R.C. Powell, J.E. Greene, Appl. Phys. Lett. 60 (1992) 2491.
[43] S. Strite, D. Chrandraeskhar, D.J. Smith, J. Sariel, H. Chen, N. Teraguchi, H. Morkoc, J. Crystal Growth 127 (1993) 204.
[44] HD. Vogel, P. Krüger, J. Pollmann, Phys. Rev. B 55 (1997) 12836.
[45] V. Serin, C. Colliex, R. Brydson, S. Matar, F. Boucher, Phys. Rev. B 58 (1998) 5106.
[46] A.F. Wright, J.S. Nelson, Appl. Phys. Lett. 66 (1995) 25.
[47] N.E. Christensen, I. Gorczyca, Phys. Rev. B 50 (1994) 4397.
[48] M. van Schilfgaarde, A. Sher, A.-B. Chen, J. Crystal Growth 178 (1997) 8–11.
[49] Numerical Data and Functional Relationships in Science and Technology, in: O. Madelung, M. Schulz, H. Weiss Landolt-Börnstein (Eds.), New Series, Group III, vol. 17(Pt. A), Springer, Berlin, 1982.
[50] H. Hei, A. Zunger, Phys. Rev. B 57 (1998) 9883–9888.
[51] A. Mäder, A. Zunger, Phys. Rev. B 51 (1995) 10462–10476.
[52] S. Yamaguchi, M. Kariya, S. Nitta, T. Takcuchi, C. Weltzel, H. Amano, I. Akasaki, Appl. Phys. Lett. 76 (2000) 876.
[53] V. Yu. Davydov, A.A. Klochikhin, R.P. Scisyan, V.V. Emtsev, S.V. Ivanov, F. Bechstedt, J. Furthmüller, H. Harima, A.V. Mudriy, Phys. Status Solidi B 229 (2002) R1.
[54] S. Wei, L.G. Ferreira, J.E. Bernard, A. Zunger, Phys. Rev. B 42 (1990) 9622.
[55] M.S. Hybertsen, S.G. Louie, Phys. Rev. B 37 (1988) 2733; X. Zhu, S.G. Louie, Phys. Rev. B 43 (1991) 14142.
[56] A. Zaoui, M. Ferhat, B. Khelifa, J.P. Dufour, H. Aourag, Phys. Stat. Sol (B) 185 (1994) 163.
[57] L. Pauling, The Nature of the Chemical Bond, Cornell University Press, New York, 1960.
[58] B. Soudini, H. Aourag, B. Khelifa, Phys. Stat. Sol. B 167 (1991) 139.
[59] K. Saarinen, P. Hautojärvi, J. Keinonen, E. Rauhala, J. Räisänen, C. Corbel, Phys. Rev. B 43 (1991) 4249.